

RESEARCH

Open Access



Dynamic displacement estimation and modal analysis of long-span bridges integrating multi-GNSS and acceleration measurements

Yanbo Niu¹, Jun Li¹, Shukang Zhou¹, Gaoyang Liu¹, Yiqiang Xiang¹, He Zhang¹ and Jiangpeng Shu^{1,2*}

Abstract

Compared with acceleration-based modal analysis, displacement can provide a more reliable and robust identification result for output-only modal analysis of long-span bridges. However, the estimated displacements from acceleration records are frequently unavailable due to unrealistic drifts. Aiming at obtaining more accurate and stable results for determining the modal parameters, this study develops a multi-rate weighted data fusion approach for estimating displacement responses in dynamic monitoring of structures based on global navigation satellite system (GNSS) and acceleration measurements. The approach initially derives the local estimations from displacement and acceleration sensors via a Kalman filter algorithm with colored measurement noise, and later uses a weighted fusion criterion of scalar linear minimum variance to fuse the results of local estimations. Then, structural modal parameters are identified by employing data-driven stochastic subspace identification (SSI) algorithm. The proposed approach is validated in a four degree-of-freedom numerical model and then applied to a long-span bridge in engineering practice. The results illustrate that the proposed approach can reduce the error of GNSS-obtained displacement and expand recognizable frequency range by introducing dynamic displacement component from acceleration measurement.

Keywords Displacement estimation, Output-only modal analysis, Data fusion, Kalman filter, Long-span bridge, GNSS

Introduction

With the rapid development of new technologies and materials, a substantial number of long-span bridges have sprung up, e.g. Russky Bridge, Sutong Bridge, Hongkong-Zhuhai-Macau Bridge etc. These bridges are generally flexible and sensitive to ambient excitations such as wind, traffic, tidal currents, and their combination. Therefore, monitoring the dynamic deformation in these structures under ambient excitations via using field measurement

techniques is an extremely important task. Excessive deformation can cause structural damage and or even destruction [1–3].

At present, accelerometer is widely employed as an effective monitoring technique to derive the dynamic responses of bridges [4–6]. It has the advantages of high measurement accuracy, high sampling frequency and good sensitivity. However, the displacement information obtained by carrying out the operation of double integral to the acceleration signal will deviate from the true value, which is difficult to meet the requirements of displacement measurement accuracy [7, 8]. Subsequently, the emergence of GPS (Global Positioning System) overcomes this problem better. GPS can monitor the three-dimensional coordinate information of bridges for all-weather in real time. Real Time Kinematic (RTK) is

*Correspondence:

Jiangpeng Shu
jpshu@zju.edu.cn

¹ College of Civil Engineering and Architecture, Zhejiang University, Hangzhou 310058, P. R. China

² Innovation Center of Yangtze River Delta, Zhejiang University, Hangzhou, China

a positioning method based on the carrier phase double difference model, which is an important development to aid GPS real-time dynamic measurement [9]. Especially, the advent of multi-constellation Global Navigation Satellite System (multi-GNSS) makes this technique get a better development. Nevertheless, it is noteworthy that GNSS sensors are insensitive to the high frequency vibration of structures, and it is difficult to track the target even with high sampling rate. Meanwhile, the existence of various error sources, including troposphere delay, ionosphere delay, troposphere error, satellite clock difference, multipath effect, etc., results in the limited positioning accuracy of GNSS. Although several errors can be eliminated in RTK mode, the multipath effect is still a main problem to be addressed for GNSS-RTK measurement.

Considering GNSS and accelerometer sensors have their own advantages and disadvantages, an integrated approach can be employed to increase the accuracy of the monitoring system. In this context, Smyth and Wu [10] put forward a multi-rate Kalman filtering approach to fuse acceleration and displacement data sampled at different frequencies. They demonstrated that the proposed algorithm can accurately estimate the displacement and velocity from noise contaminated measurements of displacement and acceleration via various numerical examples. Enlightened by this study, Kim et al. [11] presented a new algorithm of the multi-rate Kalman filtering via introducing acceleration measurement bias. Experimental verification was that the proposed algorithm can improve the accuracy of displacement estimation compared with reference in the previous literature [10]. Subsequently, Xu et al. [12] proposed a novel step of employing maximum likelihood estimation (MLE) to determine the necessary noise parameters required by the Kalman filter algorithm. Their study validated that MLE is an effective method for accurately estimating the noise parameters of measurement signals via a numerical example and a field measurement test. In the aforementioned studies, the correlated process and measurement noises were deemed to white Gaussian noises. However, this assumption does not in accordance with the general case. Hence it can only derive the suboptimal fusion estimation. Previous studies have indicated that the multipath error is the main factor affecting the positioning accuracy of GNSS-RTK sensors, which is mainly distributed in the low frequency range of GNSS signal [13]. Furthermore, Górski [14] has verified that the low frequency background noise of GNSS sensors does not follow Gaussian distribution via a stability test. Due to the vibration forms of a large number of long-span bridges belong to low frequency vibration, the low frequency noise of GNSS has a more significant influence on monitoring results than that of high frequency noise. Based on the above-mentioned analysis, considering the influence

of colored measurement noise, incorporating dynamic displacement from acceleration into GNSS-derived displacement can be seen promising in achieving accurate displacement measurement.

An principal goal of accurate displacement measurement is to extract structural modal parameters (i.e. natural frequencies, mode shapes and damping ratios). These parameters are important indicators for evaluating the safety and stability performances of bridges [15–17]. They are bound up with material characteristics, structural stiffness, mass distribution, foundation types, etc., hence their predictions are sophisticated. Nowadays, the frequently used methods for modal parameter identification can be divided into two types, i.e. traditional modal analysis (TMA) [18, 19] and operational modal analysis (OMA) [20–22] methods. TMA requires to measure excitation forces and responses of structures simultaneously. This method needs expensive excitation equipment and requires interrupting the normal operation of structures. Moreover, artificial excitation is often applied to the local position of the structure, which can easily cause damage to the structure. Whereas OMA can identify the modal parameters of the structure without artificial excitation and only rely on the response information of the structure, hence, this method is used more often [23–25]. Based on accurate displacement measurement, the OMA method is used to accurately extract structural modal parameters, which is an important task in structural health monitoring (SHM) for long-span bridges.

Inspired by the above research, this study presents a multi-rate weighted data fusion approach with colored measurement noise for estimating displacement responses of long-span bridges under operational conditions. The developed approach can derive a high-sampling rate displacement with improved accuracy via fusing the GNSS signal and the acceleration signal. Compared with the structural modes extracted by GNSS-derived displacement, higher-order modes can be determined from the estimated displacement. A numerical model and a practical bridge test are conducted to verify the performance of the developed approach.

Methodology

This study develops a multi-rate data fusion approach, as illustrated in Fig. 1. This approach involves two parts: (1) Local estimation: the Kalman filter algorithm with colored measurement noise is used to derive the results of local estimation of each sensor. (2) Fusion estimation: a weighted fusion criterion of scalar linear minimum variance is employed to fuse the local estimations for obtaining accurate displacement measurement. Then, structural modal parameters are determined by using data-driven stochastic subspace identification (SSI) algorithm based on accurate displacement measurement.

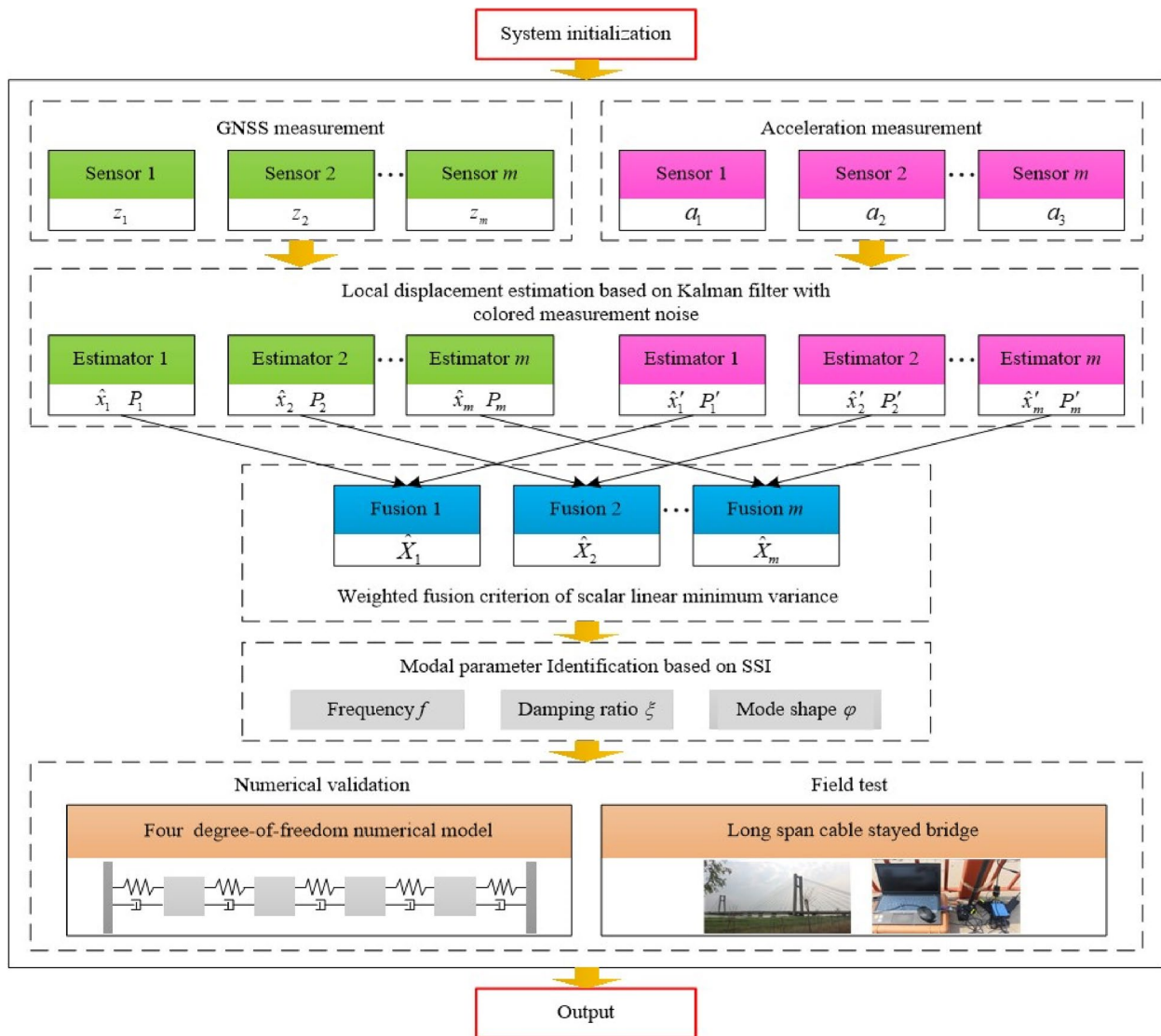


Fig. 1 Flow chart of displacement estimation and operational modal analysis based on data fusion and SSI algorithms

Displacement estimated based on data fusion

This section presents the proposed data fusion approach based on the Kalman filter with colored measurement noise. The presence of colored noise is likely to lead to incorrect analysis of bridge deformation signals and affect the estimation of modal parameter [26, 27]. Ignoring the impact of colored noise may degrade the performance of identification algorithms [28].

Assuming that the sampling interval of acceleration is T_a , and the sampling interval of displacement is T_d . They have the following relationship, i.e., $T_d/T_a = M$. β_d and β_a the associated measurement noise of displacement and acceleration with covariance r and q ; $\beta_d \sim N(0 \ \mathbf{R})$; $\beta_a \sim N(0 \ \mathbf{Q})$; $\mathbf{Q} = \begin{bmatrix} 0 & 0 \\ 0 & q \end{bmatrix}$; $\mathbf{R} = r$. The measurement process can be modeled by using the following equation:

$$\begin{cases} \mathbf{x}_k = \mathbf{A}\mathbf{x}_{k-1} + \mathbf{B}\mathbf{a}_{k-1} + \boldsymbol{\omega}_{k-1} \\ \mathbf{z}_k = \mathbf{H}\mathbf{x}_k + \boldsymbol{\eta}_k \end{cases} \quad (1)$$

where $\mathbf{A} = \begin{bmatrix} 1 & T_a \\ 0 & 1 \end{bmatrix}$; $\mathbf{B} = \begin{bmatrix} T_a^2/2 \\ T_a \end{bmatrix}$; $\mathbf{H} = [1 \ 0]$; $\boldsymbol{\omega}_k$ and $\boldsymbol{\eta}_k$ are uncorrelated white noise sequences with zero mean value, which satisfy the following conditions:

$$\begin{cases} \mathbf{Q}_k = E(\boldsymbol{\omega}_k \boldsymbol{\omega}_k^T) = q \begin{bmatrix} T_a^2/2 & T_a^3/2 \\ T_a^2/2 & T_a \end{bmatrix} \\ \mathbf{R}_k = E(\boldsymbol{\eta}_k \boldsymbol{\eta}_k^T) = \frac{\mathbf{R}}{T_a} \end{cases} \quad (2)$$

where \mathbf{Q}_k and \mathbf{R}_k are the variance matrix of system noise and measurement noise respectively. The whole process

of the traditional Kalman filtering can be described as the following five equations [26, 27]:

$$\begin{cases} \hat{\mathbf{x}}_{k|k-1} = \mathbf{A}\hat{\mathbf{x}}_{k-1|k-1} \\ \mathbf{P}_{k|k-1} = \mathbf{A}\mathbf{P}_{k-1|k-1}\mathbf{A}^T + \mathbf{Q}_{k-1} \\ \mathbf{K}_k = \mathbf{P}_{k|k-1}\mathbf{H}^T[\mathbf{H}\mathbf{P}_{k|k-1}\mathbf{H}^T + \mathbf{R}_k]^{-1} \\ \hat{\mathbf{x}}_{k|k} = \hat{\mathbf{x}}_{k|k-1} + \mathbf{K}_k[\mathbf{z}_k - \mathbf{H}\hat{\mathbf{x}}_{k|k-1}] \\ \mathbf{P}_{k|k} = [\mathbf{I} - \mathbf{K}_k\mathbf{H}]\mathbf{P}_{k|k-1} \end{cases} \quad (3)$$

where $\hat{\mathbf{x}}_{k|k-1}$ is the prior estimation; $\hat{\mathbf{x}}_{k-1|k-1}$ is the posteriori estimation; \mathbf{P}_{k-1} is the state error covariance matrix; \mathbf{K}_k is the Kalman filter gain matrix; If the initial values of $\hat{\mathbf{x}}_0$ and \mathbf{P}_0 are known, the system state $\hat{\mathbf{x}}_k$ can be estimated via employing the measured value \mathbf{z}_k . If the measurement noise $\boldsymbol{\eta}_k$ is of a colored noise, $\text{cov}(\boldsymbol{\eta}_k, \boldsymbol{\eta}_j) \neq 0 (k \neq j)$. In this case, $\boldsymbol{\eta}_k$ in Eq. (1) can be expressed as [29, 30]:

$$\boldsymbol{\eta}_k = \boldsymbol{\psi}_{k-1}\boldsymbol{\eta}_{k-1} + \boldsymbol{\zeta}_{k-1}, \quad \boldsymbol{\zeta}_k \sim N(0, \mathbf{R}_k) \quad (4)$$

where $\boldsymbol{\psi}_k$ is the measurement noise transfer matrix. The pseudo-measurement is introduced to whiten the colored measurement noise, as follows:

$$\mathbf{y}_k = \mathbf{z}_{k+1} - \boldsymbol{\psi}_k\mathbf{z}_k = \mathbf{C}_k\mathbf{x}_k + \mathbf{v}_k \quad (5)$$

$$\begin{cases} E(\mathbf{v}_k\mathbf{v}_j^T) = \bar{\mathbf{R}} \\ E(\boldsymbol{\omega}_k\mathbf{v}_j^T) = \mathbf{Q}_k\mathbf{H}^T \end{cases} \quad (6)$$

where $\mathbf{C}_k = \mathbf{H}\mathbf{A} - \boldsymbol{\psi}_k\mathbf{H}$; $\mathbf{v}_k = \mathbf{H}\boldsymbol{\omega}_k + \boldsymbol{\zeta}_k$; $\bar{\mathbf{R}}_k = \mathbf{H}\mathbf{Q}_k\mathbf{H}^T + \mathbf{R}_k$. The decorrelation analysis method can be used to filter out the correlation between stochastic noise and measurement noise [30], as follows:

$$\begin{aligned} \mathbf{x}_k &= \mathbf{A}\mathbf{x}_{k-1} + \boldsymbol{\omega}_{k-1} + \mathbf{J}_{k-1}(\mathbf{y}_{k-1} - \mathbf{C}_{k-1}\mathbf{x}_{k-1} - \mathbf{v}_{k-1}) \\ &= \mathbf{D}_{k-1}\mathbf{x}_{k-1} + \mathbf{J}_{k-1}\mathbf{y}_{k-1} + \boldsymbol{\mu}_{k-1} \end{aligned} \quad (7)$$

$$\begin{cases} E(\boldsymbol{\mu}_k\boldsymbol{\mu}_j^T) = \bar{\mathbf{Q}}_k \\ E(\boldsymbol{\mu}_k\mathbf{v}_j^T) = \mathbf{Q}_k\mathbf{H}^T - \mathbf{J}_k\bar{\mathbf{R}}_k \end{cases} \quad (8)$$

where $\bar{\mathbf{Q}}_k = \mathbf{Q}_k + \mathbf{J}_k\bar{\mathbf{R}}_k\mathbf{J}_k^T - \mathbf{Q}_k\mathbf{H}^T\mathbf{J}_k^T - \mathbf{J}_k\mathbf{H}\mathbf{Q}_k$; $\mathbf{D}_k = \mathbf{A} - \mathbf{J}_k\mathbf{C}_k$; $\boldsymbol{\mu}_{k-1} = \boldsymbol{\omega}_{k-1} - \mathbf{J}_k\mathbf{v}_k$.

To make $E(\boldsymbol{\mu}_k\mathbf{v}_j^T)$ is equal to zero, it requires:

$$\mathbf{J}_k = \mathbf{Q}_k\mathbf{H}^T(\bar{\mathbf{R}}_k)^{-1} \quad (9)$$

After the above treatment, we can get the new state space model:

$$\begin{cases} \mathbf{x}_k = \mathbf{D}_{k-1}\mathbf{x}_{k-1} + \mathbf{J}_{k-1}\mathbf{y}_{k-1} + \boldsymbol{\mu}_{k-1} & \boldsymbol{\mu}_{k-1} \sim N(0, \bar{\mathbf{Q}}_k) \\ \mathbf{y}_k = \mathbf{C}_k\mathbf{x}_k + \mathbf{v}_k & \mathbf{v}_{k-1} \sim N(0, \bar{\mathbf{R}}_k) \end{cases} \quad (10)$$

Then, the Kalman filter algorithm with colored measurement noise can be described as:

Time update:

$$\begin{cases} \hat{\mathbf{x}}_{k|k-1} = \mathbf{D}_{k-1}\hat{\mathbf{x}}_{k-1|k-1} + \mathbf{J}_{k-1}\mathbf{y}_{k-1} \\ \mathbf{P}_{k|k-1} = \mathbf{D}_{k-1}\mathbf{P}_{k-1|k-1}\mathbf{D}_{k-1}^T + \mathbf{Q}_{k-1} \end{cases} \quad (11)$$

Measurement update:

$$\begin{cases} \hat{\mathbf{x}}_{k|k} = \hat{\mathbf{x}}_{k|k-1} + \mathbf{C}_k[\mathbf{y}_k - \mathbf{C}_k\hat{\mathbf{x}}_{k|k-1}] \\ \mathbf{P}_{k|k} = [\mathbf{I} - \mathbf{K}_k\mathbf{C}_k]\mathbf{P}_{k|k-1} \end{cases} \quad (12)$$

Kalman gain matrix:

$$\mathbf{K}_k = \mathbf{P}_{k|k-1}\mathbf{C}_k^T[\mathbf{C}_k\mathbf{P}_{k|k-1}\mathbf{C}_k^T + \bar{\mathbf{R}}_k]^{-1} \quad (13)$$

Note that the measured displacements are unavailable between the times kT_d , only the time update based on Eq. (11) is performed. When the measured displacements are available at times kT_d , both the time update and measurement update should be performed.

Thus, a series of local estimations are derived (i.e., displacement: $\hat{\mathbf{X}}_{1,k|k}, \hat{\mathbf{X}}_{2,k|k}, \dots, \hat{\mathbf{X}}_{M,k|k}$; and covariance: $\mathbf{P}_{1,k|k}, \mathbf{P}_{2,k|k}, \dots, \mathbf{P}_{M,k|k}$). If the local estimation errors are uncorrelated, the optimal fusion estimation results $\hat{\mathbf{X}}_{k|k}$ can be derived via using a weighted fusion criterion of scalar linear minimum variance. It can be written as:

$$\hat{\mathbf{X}}_{k|k} = \alpha_1\hat{\mathbf{X}}_{1,k|k} + \alpha_2\hat{\mathbf{X}}_{2,k|k} + \dots + \alpha_j\hat{\mathbf{X}}_{j,k|k} + \dots + \alpha_M\hat{\mathbf{X}}_{M,k|k} \quad (14)$$

where $\hat{\mathbf{X}}_{j,k|k}$ is the local estimation value obtained after Kalman filter by the j -th sensor; α_j is the weight coefficient, which can be expressed in the following form:

$$\alpha_j = \rho / \text{tr}\mathbf{P}_{j,k|k} \quad (15)$$

where $\rho = \left(\frac{1}{\text{tr}\mathbf{P}_{1,k|k}} + \frac{1}{\text{tr}\mathbf{P}_{2,k|k}} + \dots + \frac{1}{\text{tr}\mathbf{P}_{j,k|k}} + \dots + \frac{1}{\text{tr}\mathbf{P}_{M,k|k}}\right)^{-1}$. The corresponding covariance matrix $\mathbf{P}_{0,k|k}$ of the estimation error has the following form:

$$\mathbf{P}_{0,k|k} = \alpha_1\mathbf{P}_{1,k|k} + \alpha_2\mathbf{P}_{2,k|k} + \dots + \alpha_j\mathbf{P}_{j,k|k} + \dots + \alpha_M\mathbf{P}_{M,k|k} \quad (16)$$

Operational modal analysis algorithm

The SSI is a widely used OMA approach for estimating structural modal parameters because it combines a good robustness and a high estimation accuracy [31, 32]. It is divided into two sub methods, i.e. data-driven SSI and covariance-driven SSI. In particular, data-driven SSI can identify modal parameters directly from the measured data, unlike covariance-driven SSI where one needs to derive the covariance matrix relating all of the measured outputs. Hence, data-driven SSI approach is employed in this study. Its basic principle (shown in Fig. 2) can

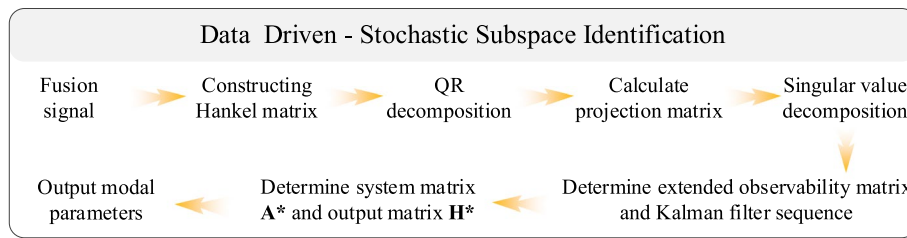


Fig. 2 The working principle of data-driven SSI

consult the literature [33, 34]. Once the system matrix A^* and output matrix H^* of state-space model of a structure are determined, the modal frequency and damping ratio can be identified by conducting eigenvalue decomposition of matrix A^* while the mode shape coefficients can be derived by the eigenvectors multiplied based on matrix H^* .

The eigenvalue decomposition of matrix A^* can be expressed as:

$$A^* = \Phi \Lambda \Phi^{-1} \tag{17}$$

$$M = \begin{bmatrix} 1 & & & \\ & 2 & & \\ & & 3 & \\ & & & 4 \end{bmatrix}, \quad K = \begin{bmatrix} 800 & -800 & 0 & 0 \\ -800 & 2400 & -1600 & 0 \\ 0 & -1600 & 4000 & -2400 \\ 0 & 0 & -2400 & 5600 \end{bmatrix}, \quad C = \alpha M + \beta K$$

where Φ is eigenvector matrix in discrete time. $\Lambda = \text{diag}(\lambda)$, λ is the eigenvalue in discrete time. It is related to the eigenvalue λ_c in continuous time, as follows:

$$\lambda_c = \frac{\ln(\lambda)}{\Delta t} \tag{18}$$

The modal frequency f and damping ratio ξ can be computed as:

$$f = \frac{\sqrt{\text{Re}^2(\lambda_c) + \text{Im}^2(\lambda_c)}}{2\pi} \tag{19}$$

$$\xi = -\frac{\text{Re}(\lambda_c)}{2\pi f} \tag{20}$$

The corresponding mode shape φ is computed as:

$$\varphi = H^* \cdot \Phi \tag{21}$$

Preliminary validation of proposed approach on numerical model

The purpose of this section is to evaluate the performance of the proposed data fusion algorithm with a simplified numerical model. Considering a four-DOF linear time-invariant spring-mass-damper model (shown in Fig. 3):

Assume that the basic parameters of this model are

The damping factors for mass proportional damping were set to $\alpha = 0.1$, $\beta = 0$. Colored noise was employed to excite the model with four-DOF. The responses of displacement and acceleration of the model were derived via using Newmark method, as shown in Fig. 4(a) and (b). The sample rate is taken as 50 Hz for measured displacement and 100 Hz for measured acceleration. This displacement obtained directly from the model is the real displacement of the system. It can be used as the reference to evaluate the working performance of the proposed approach. To simulate the field measurement data, a colored noise is added into the true displacement and acceleration responses. First, a Gaussian white noise with signal-to-noise ratio (SNR) of 5 dB is generated. Then, a shaping filter is designed to filter the generated white noise to derive a colored

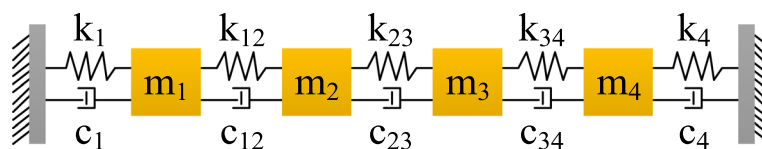


Fig. 3 Four degree-of-freedom linear spring-mass-damper model

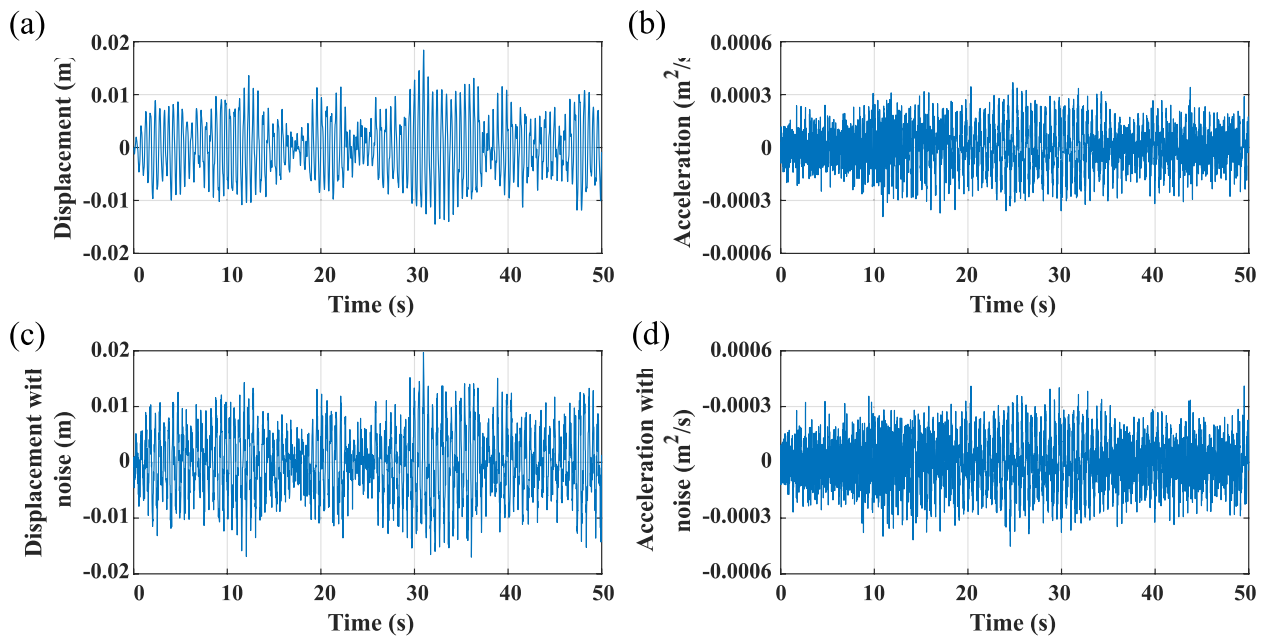


Fig. 4 Displacement and acceleration of a four-DOF model under colored noise excitation: (a) original displacement response; (b) original acceleration response; (c) displacement response with added noise; (d) acceleration response with added noise

noise of non-uniform power spectral density (PSD). This is a relatively weak level of noise. Figure 4(c) and (d) show the displacement and acceleration responses after adding colored noise. In particular, a comparative study was carried out to investigate the performance of the following six cases. Cases 1–3 process the simulated signal with colored noise based on the assumption of white noise, while cases 4–6 consider the impact of colored noise. The purpose of implementing these cases is, on the one hand, to reveal the influence of white noise and colored noise on the estimation results, and on the other hand, to compare the estimation accuracy of single sensor with that of multi-sensor fusion.

- Case 1: Displacement estimation was derived based on only displacement measurement by using Kalman filter method with white measurement noise;
- Case 2: Displacement estimation was derived based on only acceleration measurement by using Kalman filter method with white measurement noise.
- Case 3: Displacement estimation was derived based on combined measurements by using Kalman filter method with white measurement noise;
- Case 4: Displacement estimation was derived based on only displacement measurement by using Kalman filter method with colored measurement noise;
- Case 5: Displacement estimation was derived based on only acceleration measurement by using Kalman filter method with colored measurement noise;

- Case 6: Displacement estimation was derived based on combined measurements by using the proposed approach.

Figures 5(a)–(f) indicate the results of displacement estimation under different cases. To quantify the accuracy of the estimated results, the normalised root mean square error (NRMSE) was introduced. It can be expressed as the following form:

$$NRMSE = \frac{\sqrt{\frac{1}{n} \sum_{i=1}^n (\hat{x}_i - x_i)^2}}{\max(x_i) - \min(x_i)} \quad (22)$$

where x_i and \hat{x}_i represent the real and estimated value at time step i , n is the number of sampled data points. Table 1 lists the NRMSE values under six different cases based on Eq. (22). It can be seen that the estimated results of cases 4, 5 and 6 are better than cases 1, 2 and 3 respectively. This is mainly because the simulated signal contains colored noise. If it is processed as white noise, the estimation accuracy is relatively low. Additionally, it can be found that when the (100 Hz) acceleration data is combined with the (50 Hz) sampled displacement, the estimation results have a drastic improvement. In other words, the estimated result of multi-sensor fusion is better than that of single sensor when the measurement noise is given. Specially, the estimated result of case 6 is superior to other cases. This implies that the proposed approach is an effective method for estimating the real displacement of the system with a higher accuracy.

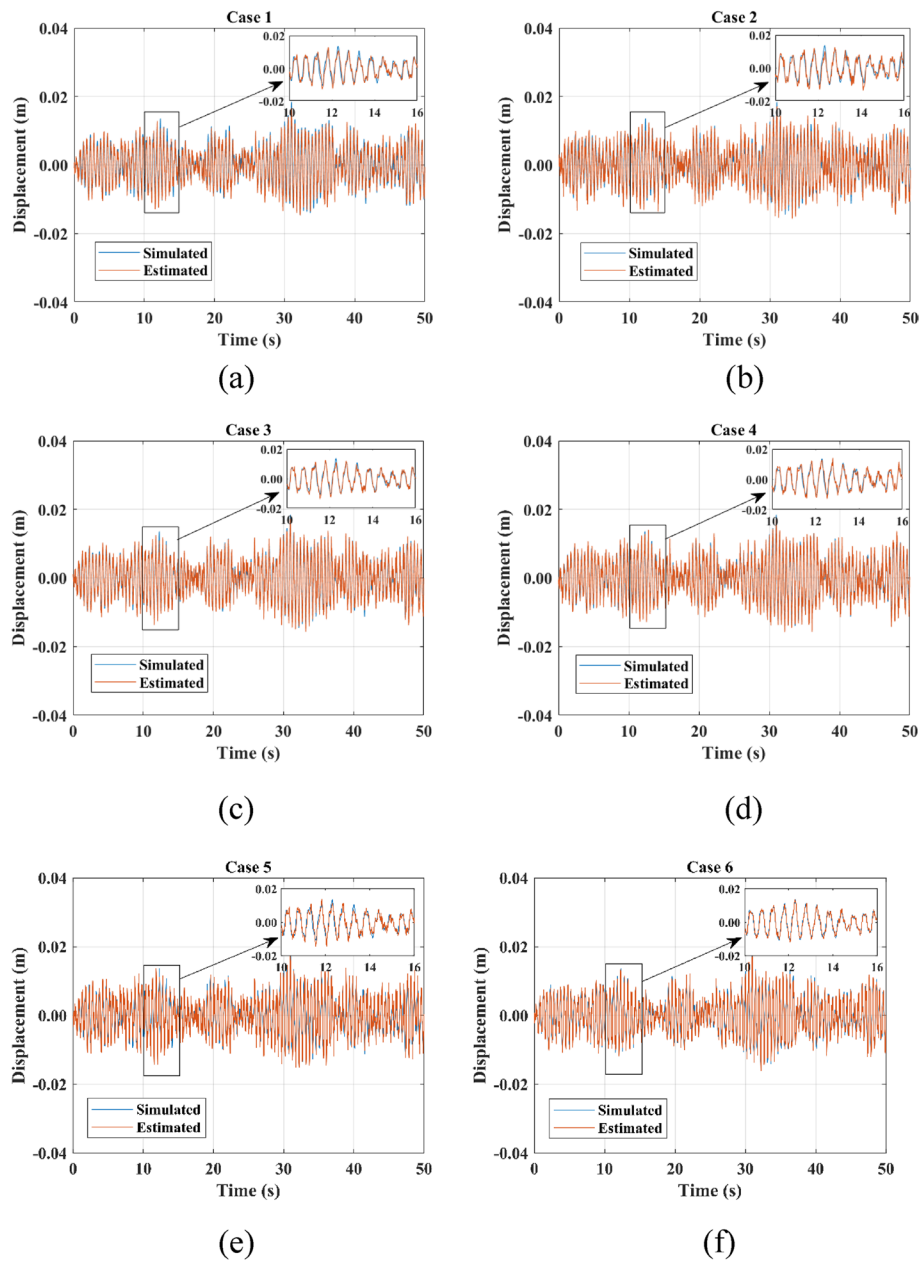


Fig. 5 Displacement estimation of a SDOF system under different cases

Table 1 NRMSE values of estimated displacements under six different cases

	Case 1	Case 2	Case 3	Case 4	Case 5	Case 6
NRMSE	0.0626	0.0667	0.0475	0.0512	0.0570	0.0320

Next, the SSI algorithm was used to calculate the modal parameters of the model. Figure 6 shows the identified mode shapes. The modal frequencies and damping ratios

were presented in Table 2. The modal assurance criterion (MAC) is used to evaluate the accuracy of mode shapes, as follows:

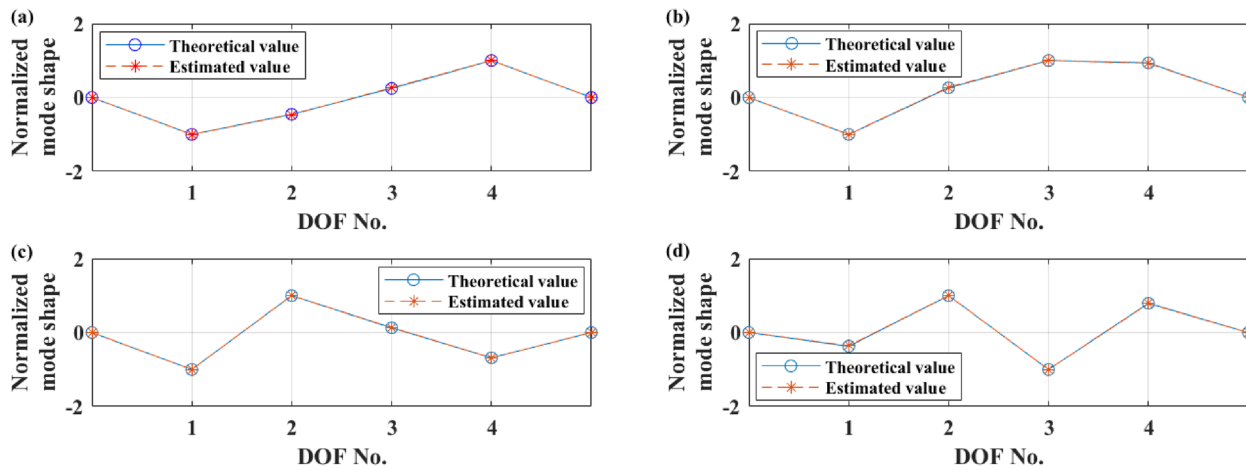


Fig. 6 Identified and theoretical mode shapes: (a) The 1st mode; (b) The 2nd mode; (c) The 3rd mode; (d) The 4th mode

Table 2 Estimated modal parameters of the numerical example

Mode	Frequency (Hz)		Damping ratio (%)		MAC
	Theoretical value	Estimated value	Theoretical value	Estimated value	
1	2.0069	2.0059	0.51	0.54	1.00
2	4.2930	4.2885	0.25	0.23	1.00
3	6.2148	6.2150	0.12	0.09	1.00
4	7.6691	7.6552	0.40	0.26	1.00

$$MAC = \frac{(\Phi_a^T \cdot \Phi_b)^2}{(\Phi_a^T \cdot \Phi_a)(\Phi_b^T \cdot \Phi_b)} \tag{23}$$

where Φ_a and Φ_b represent the theoretical and estimated mode shapes, respectively. It can be found that the results have a good agreement with the theoretical values.

Application to a long-span cable-stayed bridge

In this section, the proposed approach was applied to displacement estimation and modal identification of a long-span cable-stayed bridge named Tianjin Yonghe (shown in Fig. 7), located in Tianjin, China, from the GNSS and accelerometer monitoring data. The bridge was built in 1983 and opened to traffic at the end of 1987, and it is a pre-stressed concrete cable-stayed bridge with three-span, couple tower and couple cable. The total length of the bridge is 510 m, and the main span and each side span are 260 m and 125 m respectively. It is noted that several damage patterns, i.e. cracks at the bottom of the mid-span girder and corroded cables, were detected in 2005. Therefore, the bridge was closed and repaired between 2005 and 2007. Subsequently, the bridge was reopened to traffic at the end of 2007 with a sophisticated health monitoring system. The bridge has been in operation for



Fig. 7 Panoramic schematic of Tianjin Yonghe Bridge

approximately 15 years, and the structural modal parameters may have changed. Notably, the position accuracy of GNSS under RTK mode was limited. Therefore, before the field measurement, a stability experiment of GNSS was performed.

FE analyses of the target bridge

Before the field measurement, a Finite Element (FE) model of the bridge was established via using ANSYS 14.5 software. The purpose of establishing the FE model is to optimize the layout of the measured points and compare

it with the experimental results. In this model, there are 475 nodes and 566 elements. The bridge towers and the main girder were modelled via employing BEAM44 element. The concrete transverse beams were individually simplified as the mass element MASS21 every 2.9 m along the bridge. The stay cables were modelled via employing LINK10 element. The bridge deck was simulated via employing SHELL63 element. The main girder was modelled as floating on the main tower, and all of the towers were fixed to the ground. The longitudinal restriction effect of the rubber supports was modelled via employing COMBIN14 elements. The Young's moduli of the towers and girder are 3.55×10^{10} N/m², and their material densities are 2,550 kg/m³. The Young's modulus of the cables is 2.0×10^{11} N/m², and its material density is 7,850 kg/m³. The mass of a single concrete transverse beam is 6,932.8 kg/m³. The Young's modulus of the bridge deck is 2.85×10^{10} N/m², and its material density is 2,500 kg/m³. It is noteworthy that the status of the bridge has changed after a long time of operation. Several damage patterns, i.e. cracks at the bottom of the mid-span girder and corroded cables, were detected in 2005. Therefore, the bridge was closed and repaired between 2005 and 2007. Subsequently, the bridge was reopened to traffic at the end of 2007 with a sophisticated health monitoring system. This study established a benchmark finite element model based on the design value, and then further modified this model by using preliminary measurements. Based on the FE modal analysis results, the first to eighth vertical vibration frequencies (i.e., 0.3996 Hz, 0.5522 Hz, 0.9332 Hz, 1.0559 Hz, 1.4217 Hz, 1.5961 Hz, 1.6662 Hz and 1.7231 Hz) and the corresponding mode shapes were derived, as shown in Fig. 8(a)-(h).

Experimental scheme and measurement

Based on the FE analysis results from Fig. 8, it can be seen that the largest deformation of the bridge are presented at 1/4, 1/2 and 3/4 of the main span, and 1/2 of the side spans. The sensors arranged at these positions can effectively reveal the vibration characteristics of the structure. Therefore, this experiment used six GNSS receivers (Sampling rate: 50 Hz) and five accelerometer sensors (Sampling rate: 100 Hz) to monitor the vibration response of the bridge. One GNSS receiver was placed on a stable ground as the reference station and approximately 50 m away from the bridge, as shown in Fig. 9(a). From Fig. 9(b), five GNSS receivers in association with five accelerometers were fixed at 1/4, 1/2 and 3/4 of the main span, and 1/2 of the side spans as the rover stations. Figure 9(c) depicts the specific locations of the measuring points (i.e., C1-C5). This experiment lasted for 9 h from 9:00 a.m. to 6:00 p.m. on 12 July 2019 local time.

Data processing and analysis

In section "Preliminary validation of proposed approach on numerical model", the superiority of the proposed approach has been verified by a numerical example. This section reports the results of employing the proposed data fusion approach to the field data recorded on Tianjin Yonghe Bridge.

Figure 10 depicts the original GNSS data of Point C3, and the corresponding PSD function. It can be seen that there are two notable peaks (i.e., 0.4150 Hz and 0.5981 Hz) corresponding to the first two vertical modes of the bridge from PSD distribution. Moreover, It can also be found that the modal frequencies identified via PSD function are agree with the results of FE analysis with a little difference. Figure 11 presents the original acceleration data of Point C3, and the corresponding PSD function. It can be observed that there are five obvious peaks (i.e., 0.4150 Hz, 0.5859 Hz, 0.9644 Hz, 1.0860 Hz and 1.4530 Hz) corresponding to the first five modal information of the bridge. In particular, it is noteworthy that Figs. 10 and 11 only show the 200 s vibration response, and the corresponding PSD and the follow-up modal calculation are calculated with 1000 s sample data. From Fig. 10, there were no apparent peaks about the third to fifth modes based on GNSS data. This implies that compared with acceleration sensors, GNSS can only detect a few number of low order modes even with a high sampling rate. Theoretically, the GNSS measurement has the chance to detect the higher vertical modes but in fact it has failed to do so. This is mainly because the positioning accuracy of GNSS is limited while the dynamic component of displacement is relatively small and easily contaminated by the measurement noise.

Next, the proposed multi-rate weighted data fusion approach was used to fuse the GNSS and acceleration data. However, it is worth noting that the measured GNSS data includes not only the dynamic part of displacement but also the quasi-static part. This study mainly focused on investigating the dynamic displacements of bridges under ambient excitation. Hence, a second-order type 1 Chebyshev high-pass digital filter with the cut-off frequency of 0.05 Hz was first adopted to remove the quasi-static part of displacement. Then, the remained dynamic part of GNSS and acceleration were fused via the developed approach. In addition, previous studies have proved that smoothing can produces a much better estimation after fusion [10, 35]. Therefore, a smoothing technique named Savitzky-Golay (SG) approach was used in this section [36]. The SG approach was a data smoothing approach depended on local least-squares polynomial approximation. It has been demonstrated that least-squares smoothing reduces noise while ensuring the height and shape of waveform peaks [37].

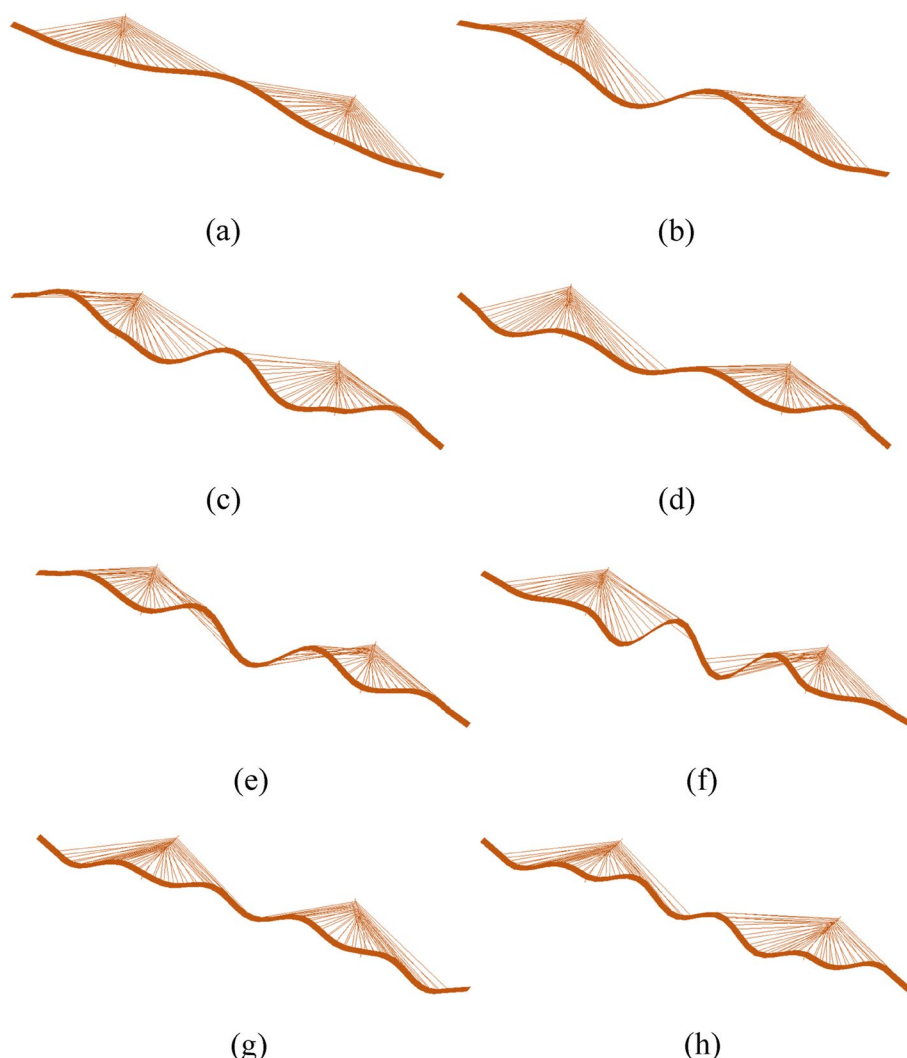


Fig. 8 Finite element modal analysis results of the Bridge: (a) The 1st mode; (b) The 2nd mode; (c) The 3rd mode; (d) The 4th mode; (e) The 5th mode; (f) The 6th mode; (g) The 7th mode; (h) The 8th mode

The final estimated displacements from GNSS, acceleration and data fusion and their PSD functions were illustrated in Fig. 12. It can be found that the estimated result based on GNSS data can identify first three modes of the bridge, but before that, only the first two modes can be detected. This implies that the filtering and smoothing approaches reduce the noise and make the dynamic components of GNSS clear. However, it was still failed to extract the fourth and fifth modes of the bridge. From Fig. 12(b), it was also seen that five distinct modes were identified via using the developed data fusion approach. Furthermore, the identified results of modal frequencies were consistent with the acceleration-derived displacement. To some extent, the problem that GNSS is insensitive to high frequency vibration of structures is alleviated. Note that the sampling rate of the estimated

displacement via using the proposed approach is 100 Hz. The standard deviations of three different estimation results were calculated (i.e., GNSS-derived displacement: 0.0104 m; Acceleration-derived displacement: 0.0101 m; Data fusion-derived displacement: 0.0089 m).

The data-driven SSI algorithm is performed on the estimated displacements. The modal frequencies and the corresponding damping ratios were listed in Table 3. It can be seen that the modal frequencies identified via GNSS-derived displacement, acceleration-derived displacement and data fusion-derived displacement are consistent. However, there is a large deviation in the damping identification results. The accurate estimation of damping is difficult because the bridge contains several sources of energy dissipation, and their lesser known combinations. Figure 13 illustrates the extracted results of the mode

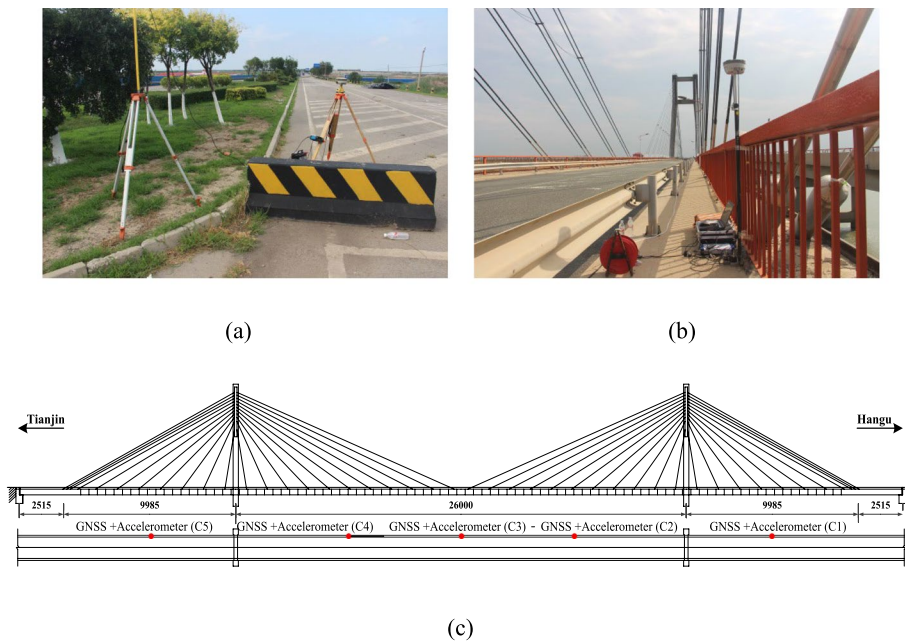


Fig. 9 Schematic figure for the field measurement: (a) GNSS reference station; (b) GNSS rover station and accelerometer sensor; (c) The position of measuring points

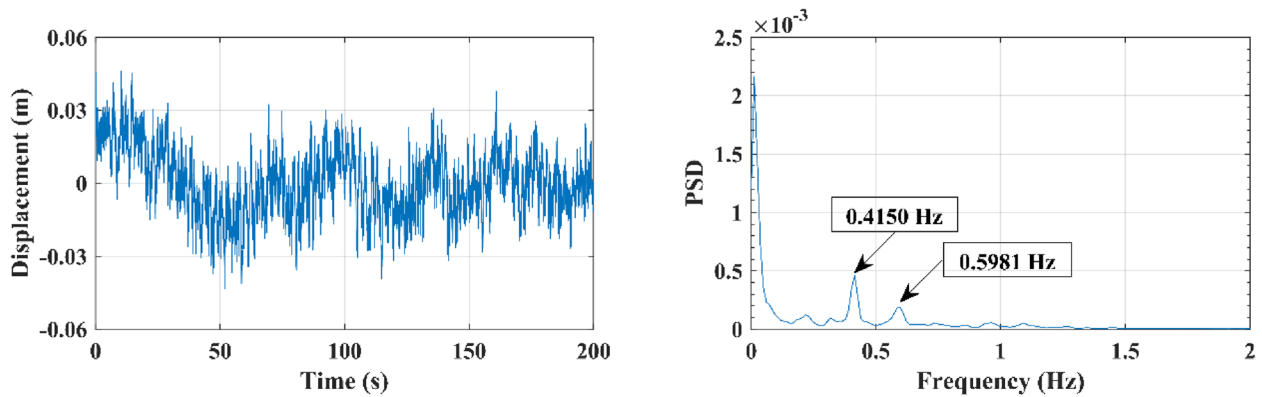


Fig. 10 GNSS signal and its PSD function

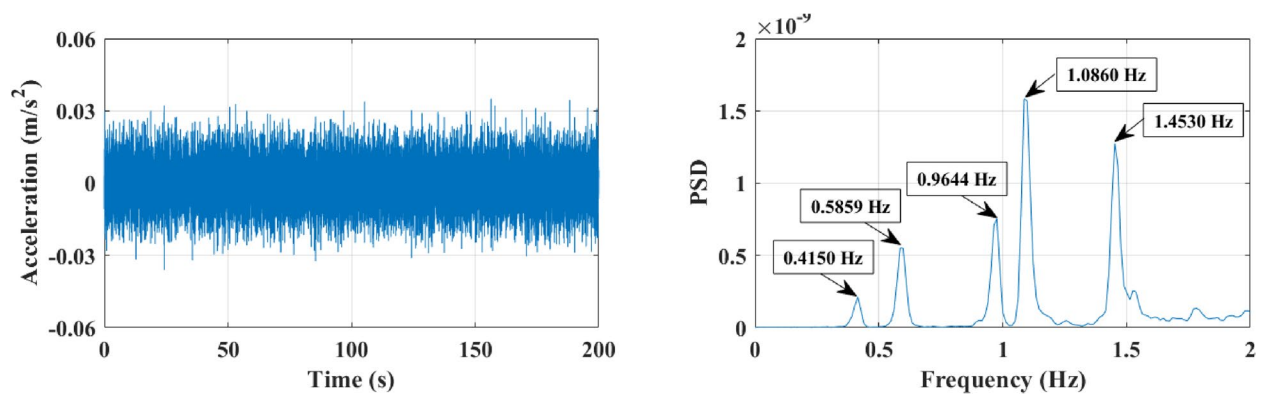


Fig. 11 Acceleration signal and its PSD function

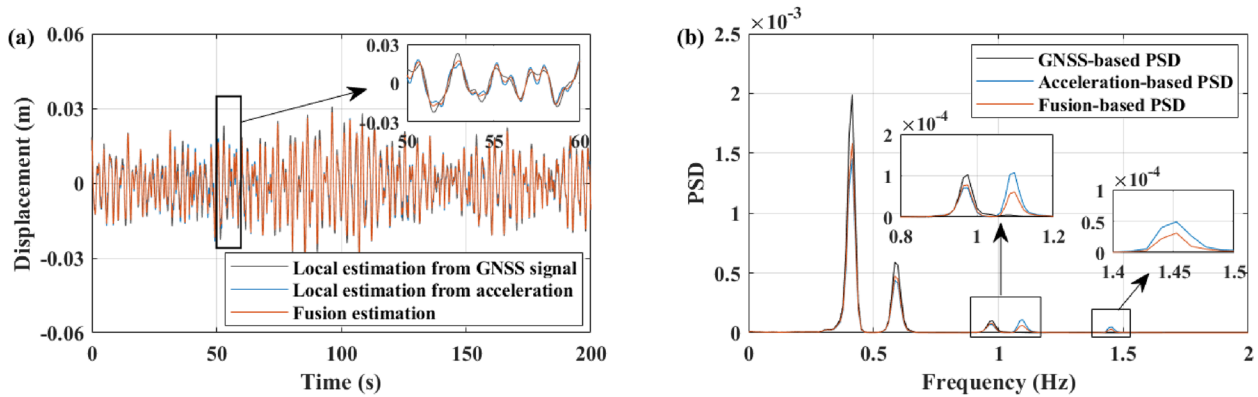


Fig. 12 Estimated displacements and the corresponding PSD functions

Table 3 Estimated modal parameters for Tianjin Yonghe Bridge based on field measurement

Mode	Frequency (Hz)				Damping ratio (%)		
	FE model	GNSS	Acceleration	Data fusion	GNSS	Acceleration	Data fusion
1	0.3996	0.4150	0.4152	0.4152	1.53	1.46	1.38
2	0.5522	0.5981	0.5860	0.5862	1.26	1.22	1.20
3	0.9332	0.9643	0.9644	0.9640	1.08	0.91	0.95
4	1.0559	–	1.0855	1.0853	–	0.86	0.90
5	1.4217	–	1.4533	1.4536	–	0.80	0.85

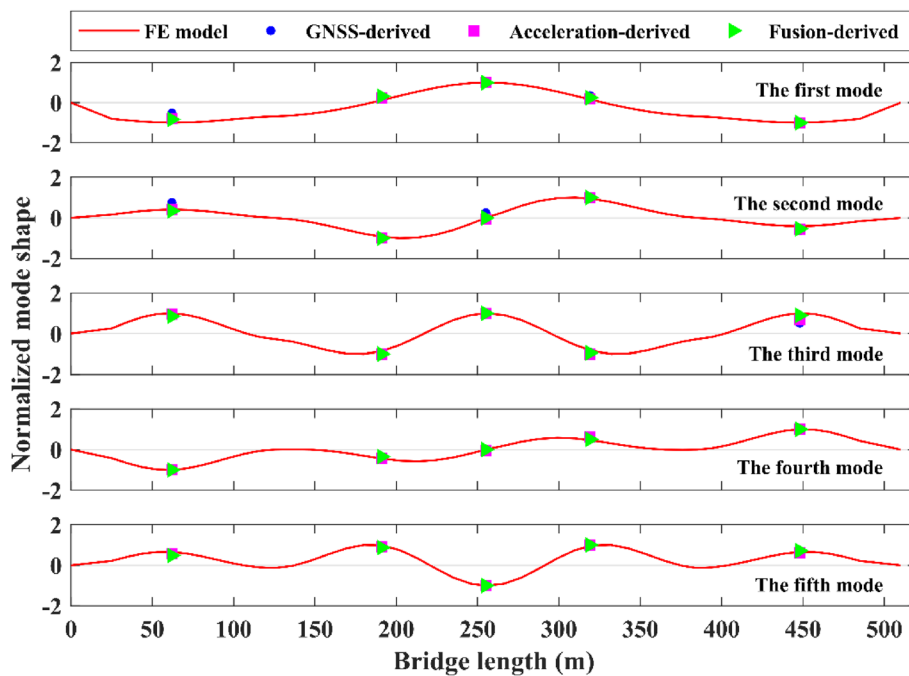


Fig. 13 Identified first five vertical mode shapes

shapes. It can be observed that the identified results are in good agreement with the theoretical values based on the FE analysis. The MAC values (shown in Table 4)

confirmed that the mode shapes identified based on data fusion-derived displacement were better than those GNSS-derived and acceleration-derived displacements.

Table 4 The MAC values of GNSS-derived, acceleration-derived and data fusion-derived displacements

Mode	MAC		
	GNSS	Acceleration	Data fusion
1	0.9016	0.9201	0.9401
2	0.9431	0.9437	0.9788
3	0.9302	0.9461	0.9759
4	–	0.9500	0.9664
5	–	0.9363	0.9625

This further proves that the developed approach has an accuracy advantage to those of the local estimations from single type sensors. Thus far, all the modal parameters of the structure were successfully obtained.

Conclusions

In this study, a multi-rate weighted data fusion approach based Kalman filter with colored measurement noise was developed to estimate dynamic displacement of a long-span bridge based on GNSS and acceleration measurements. Then, the data-driven SSI method was employed to identify modal parameters of the bridge from the estimated displacement. The method is tested using a four-DOF system and an actual long-span bridge. The following conclusions are summarized:

- The proposed data fusion approach is capable of accurately estimating structural dynamic displacements. The feasibility and effectiveness of the approach were validated by a comparative study of a spring-mass-damper model. On the premise of a given measurement noise, the estimated result of multi-sensor fusion performs better than that of single sensor. Moreover, the proposed approach with considering colored measurement noise is superior to the general approach with considering white measurement noise. The corresponding NRMSE index decreased from 0.0475 to 0.0320.
- The proposed approach can improve the accuracy of GNSS-derived displacement and expand recognizable frequency range by fusing acceleration information. Based on raw GNSS data, only the first two modes of the bridge were detected even with high sampling rate. However, the third mode of the bridge became distinct based on GNSS local estimation obtained by Kalman filtering. This is mainly because the noise reduction makes the dynamic components of displacement clear. Importantly, the fourth and fifth modes of the bridge can be extracted

if the measured displacement from GNSS was fused with acceleration information using the developed approach. In other words, the developed fusion strategy alleviates the problem of low dynamic tracking accuracy of GNSS.

- The identified modal frequencies based on GNSS-derived, acceleration-derived and data fusion-derived displacements are consistent. Meanwhile, they are in agreement with the theoretical values based on the FE analysis. Moreover, the MAC values demonstrated that the modes identified via fusion-derived displacement are better than GNSS-derived and acceleration-derived displacements. This further reveals that multi-sensor fusion has an accuracy improvement over single type of sensors.

Acknowledgements

The authors would like to gratefully acknowledge the National Natural Science Foundation of China (52108179), the China Postdoctoral Science Foundation (2021M692835) and the Key R&D Program of Zhejiang, which made the research work possible.

Authors' contributions

Yanbo Niu: conduct literature review, build models and analyse, draft the manuscript; Jun Li: provide assistance on building models; Shukang Zhou, provide assistance on the dataset; Gaoyang Liu, refine the manuscript; Yiqiang Xiang, revise the manuscript; He Zhang, reply comments; Jiangpeng Shu, envision the study. The authors reviewed and approved the final manuscript.

Funding

The financial support for this study was provided by the National Natural Science Foundation of China (52108179), the China Postdoctoral Science Foundation (2021M692835) and the Key R&D Program of Zhejiang (2023C01161).

Availability of data and materials

Data requests will be reviewed based on the corresponding author's discretion.

Declarations

Competing interests

The authors declare no competing interests.

Received: 17 January 2023 Revised: 22 March 2023 Accepted: 24 March 2023

Published online: 12 April 2023

References

1. Shu J, Ding W, Zhang J, Lin F, Duan Y (2022) Continual-learning-based framework for structural damage recognition. *Struct Control Heal Monit* 29:e3093. <https://doi.org/10.1002/stc.3093>
2. Zhao W, Liu Y, Zhang J, Shao Y, Shu J (2022) Automatic pixel-level crack detection and evaluation of concrete structures using deep learning. *Struct Control Heal Monit* 29:e2981. <https://doi.org/10.1002/stc.2981>
3. Shu J, Li J, Zhang J, Zhao W, Duan Y, Zhang Z (2022) An active learning method with difficulty learning mechanism for crack detection. *Smart Structures and Systems* 39:53–62. <https://doi.org/10.12989/sss.2022.29.1.195>
4. Piombo BAD, Fasana A, Marchesiello S, Ruzzene M (2000) Modelling and identification of the dynamic response of a supported bridge. *Mech Syst Signal Process* 14:75–89. <https://doi.org/10.1006/mssp.1999.1266>

5. Jia J, Feng S, Liu W (2015) A triaxial accelerometer monkey algorithm for optimal sensor placement in structural health monitoring. *Meas Sci Technol* 26:65104. <https://doi.org/10.1088/0957-0233/26/6/065104>
6. Gatti M (2019) Structural health monitoring of an operational bridge: a case study. *Eng Struct* 195:200–209. <https://doi.org/10.1016/j.engstruct.2019.05.102>
7. Masri SF, Sheng LH, Caffrey JP et al (2004) Application of a Web-enabled real-time structural health monitoring system for civil infrastructure systems. *Smart Mater Struct* 13:1269–1283. <https://doi.org/10.1088/0964-1726/13/6/001>
8. Moschas F, Stiros S (2011) Measurement of the dynamic displacements and of the modal frequencies of a short-span pedestrian bridge using GPS and an accelerometer. *Eng Struct* 33:10–17. <https://doi.org/10.1016/j.engstruct.2010.09.013>
9. Ince CD, Sahin M (2000) Real-time deformation monitoring with GPS and Kalman Filter. *Earth, Planets Sp* 52:837–840. <https://doi.org/10.1186/BF03352291>
10. Smyth A, Wu M (2007) Multi-rate Kalman filtering for the data fusion of displacement and acceleration response measurements in dynamic system monitoring. *Mech Syst Signal Process* 21:706–723. <https://doi.org/10.1016/j.ymssp.2006.03.005>
11. Kim J, Kim K, Sohn H (2014) Autonomous dynamic displacement estimation from data fusion of acceleration and intermittent displacement measurements. *Mech Syst Signal Process* 42:194–205. <https://doi.org/10.1016/j.ymssp.2013.09.014>
12. Xu Y, Brownjohn JMW, Hester D, Koo KY (2017) Long-span bridges: enhanced data fusion of GPS displacement and deck accelerations. *Eng Struct* 147:639–651. <https://doi.org/10.1016/j.engstruct.2017.06.018>
13. Yi T, Li H, Gu M (2010) Full-scale measurements of dynamic response of suspension bridge subjected to environmental loads using GPS technology. *Sci China Technol Sci* 53:469–479. <https://doi.org/10.1007/s11431-010-0051-2>
14. Górski P (2015) Investigation of dynamic characteristics of tall industrial chimney based on GPS measurements using random decrement method. *Eng Struct* 83:30–49. <https://doi.org/10.1016/j.engstruct.2014.11.006>
15. Shu J, Zhang C, Gao Y, Niu Y (2023) A multi-task learning-based automatic blind identification procedure for operational modal analysis. *Mech Syst Signal Process* 187:109959. <https://doi.org/10.1016/j.ymssp.2022.109959>
16. Niu Y, Ye Y, Zhao W, Duan Y, Shu J (2021) Identifying modal parameters of a multispan bridge based on high-rate GNSS-RTK measurement using the CEEMD-RDT approach. *J Bridg Eng* 26:04021049. [https://doi.org/10.1061/\(ASCE\)BE.1943-5592.0001754](https://doi.org/10.1061/(ASCE)BE.1943-5592.0001754)
17. Niu Y, Ye Y, Zhao W, Shu J (2020) Dynamic monitoring and data analysis of a long-span arch bridge based on high-rate GNSS-RTK measurement combining CFCEEMD method. *J Civ Struct Heal. Monit* 11:35–48. <https://doi.org/10.1007/s13349-020-00436-x>
18. Kalybek M, Bocian M, Pakos W, et al (2021) Performance of camera-based vibration monitoring systems in input-output modal identification using shaker excitation. *Remote Sens* 13:3471. <https://doi.org/10.3390/rs13173471>
19. Mukhopadhyay S, Luş H, Betti R (2014) Modal parameter based structural identification using input-output data: minimal instrumentation and global identifiability issues. *Mech Syst Signal Process* 45:283–301. <https://doi.org/10.1016/j.ymssp.2013.11.005>
20. Pan C, Ye X, Mei L (2021) Improved automatic operational modal analysis method and application to large-scale bridges. *J Bridg Eng* 26:04021051. [https://doi.org/10.1061/\(asce\)be.1943-5592.0001756](https://doi.org/10.1061/(asce)be.1943-5592.0001756)
21. Sun M, Makki Alamdari M, Kalthori H (2017) Automated operational modal analysis of a cable-stayed bridge. *J Bridg Eng* 22:05017012. [https://doi.org/10.1061/\(asce\)be.1943-5592.0001141](https://doi.org/10.1061/(asce)be.1943-5592.0001141)
22. Brownjohn JMW, Magalhães F, Caetano E, Cunha A (2010) Ambient vibration re-testing and operational modal analysis of the humber bridge. *Eng Struct* 32:2003–2018. <https://doi.org/10.1016/j.engstruct.2010.02.034>
23. Pereira S, Magalhães F, Cunha A et al (2021) Modal identification of concrete dams under natural excitation. *J Civ Struct Heal Monit* 11:465–484. <https://doi.org/10.1007/s13349-020-00462-9>
24. Jimenez Capilla JA, Au SK, Brownjohn JMW, Hudson E (2021) Ambient vibration testing and operational modal analysis of monopole telecoms structures. *J Civ Struct Heal Monit* 11:1077–1091. <https://doi.org/10.1007/s13349-021-00499-4>
25. Ye X, Huang P, Pan C, Mei L (2021) Innovative stabilization diagram for automated structural modal identification based on ERA and hierarchical cluster analysis. *J Civ Struct Heal Monit* 11:1355–1373. <https://doi.org/10.1007/s13349-021-00514-8>
26. Ma J (2022) BDS/GPS deformation analysis of a long-span cable-stayed bridge based on colored noise filtering. *Geod Geodyn*. <https://doi.org/10.1016/j.geog.2022.08.005>
27. Huang K, Yuen KV, Wang L (2022) Real-time simultaneous input-state-parameter estimation with modulated colored noise excitation. *Mech Syst Signal Process* 165:108378. <https://doi.org/10.1016/j.ymssp.2021.108378>
28. Lu X, He X, Chen H, ZHENG R, (2021) Operational modal parameter identification with colored noise excitation. *Chinese J Aeronaut* 34:288–300. <https://doi.org/10.1016/j.cja.2020.09.006>
29. Choi HD, Ahn CK, Lim MT (2013) Time-domain filtering for estimation of linear systems with colored noises using recent finite measurements. *Meas J Int Meas Confed* 46:2792–2797. <https://doi.org/10.1016/j.measurement.2013.03.029>
30. Chang G (2014) On kalman filter for linear system with colored measurement noise. *J Geod* 88:1163–1170. <https://doi.org/10.1007/s00190-014-0751-7>
31. Bajrić A, Høgsberg J (2018) Estimation of hysteretic damping of structures by stochastic subspace identification. *Mech Syst Signal Process* 105:36–50. <https://doi.org/10.1016/j.ymssp.2017.11.042>
32. Cancelli A, Laflamme S, Alipour A et al (2020) Vibration-based damage localization and quantification in a pretensioned concrete girder using stochastic subspace identification and particle swarm model updating. *Struct Heal Monit* 19:587–605. <https://doi.org/10.1177/1475921718820015>
33. Reynders EPB (2021) Uncertainty quantification in data-driven stochastic subspace identification. *Mech Syst Signal Process* 151:107338. <https://doi.org/10.1016/j.ymssp.2020.107338>
34. Guo J, Hu CJ, Zhu MJ, Ni YQ (2021) Monitoring-based evaluation of dynamic characteristics of a long span suspension bridge under typhoons. *J Civ Struct Heal Monit* 11:397–410. <https://doi.org/10.1007/s13349-020-00458-5>
35. Lei Y, Luo S, Su H (2018) Multi-rate data fusion based kalman filtering with unknown input for online estimation of dynamic displacements. *Earth and Space 2018: Engineering for Extreme Environments - Proceedings of the 16th Biennial International Conference on Engineering, Science, Construction, and Operations in Challenging Environments*
36. Savitzky A, Golay MJE (1964) Smoothing and differentiation of data by simplified least squares procedures. *Anal Chem*. <https://doi.org/10.1021/ac60214a047>
37. Schafer RW (2011) What is a savitzky-golay filter? *IEEE Signal Process Mag*. <https://doi.org/10.1109/MSP.2011.941097>

Publisher's Note

Springer Nature remains neutral with regard to jurisdictional claims in published maps and institutional affiliations.

Submit your manuscript to a SpringerOpen® journal and benefit from:

- Convenient online submission
- Rigorous peer review
- Open access: articles freely available online
- High visibility within the field
- Retaining the copyright to your article

Submit your next manuscript at ► [springeropen.com](https://www.springeropen.com)